Structural Relationship between Negative Thermal Expansion and Quartic Anharmonicity of Cubic ScF_{3}

Chen W. Li, Xiaoli Tang, J. A. Muñoz, J. B. Keith, S. J. Tracy, D. L. Abernathy, and B. Fultz

Phys. Rev. Lett. **107**, 195504 — Published 4 November 2011

DOI: 10.1103/PhysRevLett.107.195504

The structural relationship between negative thermal expansion and quartic anharmonicity of cubic ScF_3

Chen W. Li,[1,*] Xiaoli Tang,[1] J. A. Muñoz,[1] J. B. Keith,[1] S. J. Tracy,[1] D. L. Abernathy,[2] and B. Fultz[1]

[1]*Department of Applied Physics and Materials Science, California Institute of Technology, Pasadena, California 91125*

[2]*Neutron Scattering Science Division, Oak Ridge National Laboratory, Oak Ridge, Tennessee 37831*

Cubic scandium tri-fluoride (ScF_3) has a large negative thermal expansion over a wide range of temperature. Inelastic neutron scattering experiments were performed to study the temperature dependence of the lattice dynamics of ScF_3 from 7 to 750 K. The measured phonon densities of states (DOS) show a large anharmonic contribution with a thermal stiffening of modes around 25 meV. Phonon calculations with first-principles methods identified the individual modes in the DOS, and frozen phonon calculations showed that some of the modes with motions of F atoms transverse to their bond direction behave as quantum quartic oscillators. The quartic potential originates from harmonic interatomic forces in the DO_9 structure of ScF_3, and accounts for phonon stiffening with temperature and a significant part of the negative thermal expansion.

PACS numbers: 63.20.Ry, 78.70.Nx, 65.40.De, 63.20.D-, 64.70.kp

Nearly all materials expand when heated, so exceptions are interesting. Negative thermal expansion (NTE) of a pure phase has attracted much attention over the past twenty years, driven both by curiosity, and by opportunities to design materials with special thermal properties. For materials like face-centered cubic plutonium and Invar alloys, NTE involves electronic or magnetic excitations. Other types of NTE are structure-induced, originating from atom arrangements in the crystal [1]. Several mechanisms of NTE have been proposed, such as deformations of polyhedra, one or two-dimensional NTE caused by normal thermal expansion of anisotropic bonds, NTE induced by interstitial cations, and NTE associated with transverse motions of linkage atoms (as in Fig. 1) [2, 3]. Often NTE is anisotropic, and it usually occurs only in a small range of temperature [4]. Zirconium tungstate (ZrW_2O_8) is a notable exception [5–10]. The NTE in ZrW_2O_8 is associated with underconstrained atom sites in the crystal structure [11]. Although some of the behavior can be understood with a "quasiharmonic" model (a harmonic model with interatomic forces adapted to the bond lengths at a given temperature), anharmonic effects are expected, but the full connection between anharmonic lattice dynamics and NTE is obscured by the complexity of the structure [11]. Simplified models like a rigid square [12, 13], a 3-atom Bravais lattice [11], and a rigid structure [14] have been used to explain the "soft-phonon" NTE mechanism, but accurate lattice dynamics for materials such as ZrW_2O_8 are not easy to obtain from geometrical models.

Very recently, a surprisingly large and isotropic negative thermal expansion was discovered in cubic scandium tri-fluoride (ScF_3) by Greve *et al.* [15]. It occurs over a wide range of temperature from 10 to about 1100 K, and exceeds -1.0×10^{-5} K^{-1}. Under ambient conditions, ScF_3 has the DO_9 crystal structure of α-ReO_3, shown in Fig. 1, and is stable from 10 K to over 1600

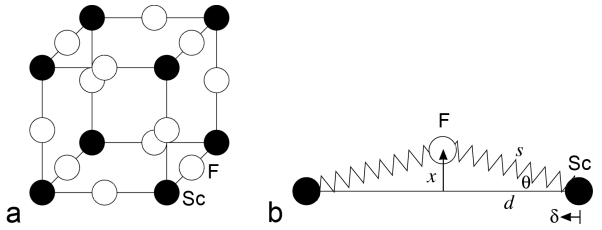

FIG. 1: (a) DO_9 structure of ScF_3. (b) Geometry and variables for the mechanical model of Sc-F bonds.

K. Although α-ReO_3 itself shows modest negative thermal expansion below 300 K [16, 17], the NTE of ScF_3 is an order of magnitude larger. Only a small amount of work has been performed on the lattice dynamics of ScF_3 [18], although materials with similar structure have been studied [19]. Here we report results from inelastic neutron scattering measurements of the lattice dynamics of ScF_3 from 7 to 750 K. The simplicity of the DO_9 structure of cubic ScF_3 allows a detailed analysis of the lattice dynamics, elucidating the connection between NTE and phonon anharmonicity.

Inelastic neutron scattering measurements were performed with ARCS, a time-of-flight Fermi chopper spectrometer at the Spallation Neutron Source at Oak Ridge National Laboratory. Coarse powders (<0.1 mm) of cubic ScF_3 crystals of 99.99% purity were loaded into annular aluminum containers with outer diameters of 30.0 mm and heights of 64.0 mm. The effective sample thickness was 2.0 mm, giving a ratio of multiply- to singly-scattered neutrons of approximately 5%. Four incident neutron energies were used, 30.0, 79.5, 118.7, and 163.0 meV. Each measurement included approximately 2×10^6 neutron counts. For temperatures of 7, 100, 200, and 300 K, the sample was mounted in a closed-cycle helium refrigerator. An electrical resistance furnace designed for vacuum service was used for temperatures of 320, 450,

600, and 750 K. Backgrounds with empty sample cans were measured at each temperature.

Data reduction was performed with the standard software package for ARCS as described previously [20, 21]. The neutron-weighted phonon density of states (DOS) curves for three incident energies are shown in Fig. 2a. Differences among the phonon DOS curves are expected from differences in instrument resolution, which improves for lower incident neutron energies. Good agreement is seen for the DOS curves measured in the refrigerator and furnace at 300 K and 320 K, showing the success of the background subtraction. Neutron diffraction patterns were obtained from the elastic scattering and used to verify the structure and lattice parameters.

All major features in the DOS broaden with temperature, indicating a decrease in phonon lifetime. To quantify thermal shifts, Gaussian functions were fitted to the five features in the phonon DOS, and Fig. 2b presents the shifts (ΔE) of the peak centers. The high-energy features 4 and 5 soften normally with temperature, but the low-energy feature 2 stiffens anomalously. Feature 3 may also stiffen, and feature 1 changes little with temperature. The shifts obtained from different incident energies agree reasonably well. Some of the features correspond to more than one phonon branch, so while the fitted shifts give a good indication of of the trend of the phonon energy changes, they usually do not pinpoint a specific mode.

First-principles calculations were performed with the local density approximation to the density functional theory, implemented in the VASP package [22]. Projector augmented wave (PAW) [23] pseudopotentials and a plane wave basis set with energy cutoff of 450 eV were used in all calculations. Within the quasi-harmonic approximation (QHA), the free energy is

$$F(T,V) = E_s(V) + \int g(\omega)\left(\frac{\hbar\omega}{2} + k_{\mathrm{B}}T\ln(1-e^{-\frac{\hbar\omega}{k_{\mathrm{B}}T}})\right)\mathrm{d}\omega \quad (1)$$

where the static energy E_s is the total energy of the crystal when all the atoms are fixed at their equilibrium positions, ω is the (angular) phonon frequency, and $g(\omega)$ is the phonon DOS for the lattice parameter, a, that minimizes $F(T, V(a))$. Here E_s was calculated self-consistently using a 4-atom primitive cell and a $12 \times 12 \times 12$ k-point grid, and phonon energies were calculated using the direct supercell method with a 108-atom supercell and a $2 \times 2 \times 2$ k-point grid. The LO-TO correction for the optical phonons was included based on the inter-plane force constants model [24].

To study anharmonic effects with VASP, we performed ab-initio Born-Oppenheimer molecular dynamics (MD) at 7, 100, 200, 300, 450, 600, and 750 K, and we also performed frozen phonon calculations. The MD simulations used a 108-atom supercell, and temperature was controlled by Nosé thermostats. For each temperature, the system was first equilibrated and then simulated for

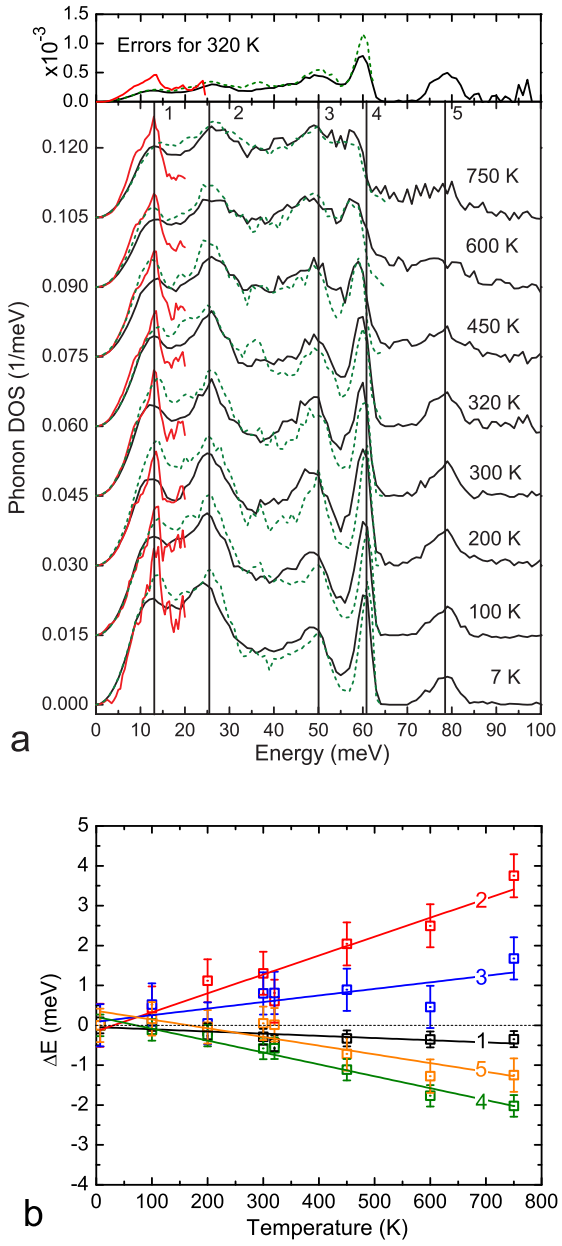

FIG. 2: (**a**) Neutron-weighted ScF_3 phonon DOS from incident energies of 118.7 meV (black), 79.5 meV (green, dashed), and 30.0 meV (red), scaled to conserve spectral areas and offset for clarity. Five vertical lines are aligned to peak centers at 7 K, and labeled by numbers. Errors at top are from counting statistics, and similar at all temperatures. (**b**) Shifts of phonon peak centers relative to 7 K data. The solid lines are linear fits. For each point, the spectrum with the best resolution was used. Error bars are mean differences between the spectra of different incident energies at all temperatures.

5 ps with a time step of 5 fs. The QHA and MD simulations were used to identify modes corresponding to experimental spectral features having anomalous temperature dependencies. The vibrational potentials of these modes were obtained through frozen phonon calculations on the minimum supercell determined by symmetry.

Figure 3 shows phonon properties calculated from first principles within the harmonic approximation. The agreement between the experimental and calculated phonon DOS curves is good after accounting for instrumental broadening and neutron weighting (neutrons are scattered about twice as efficiently from motions of Sc atoms than F atoms). All major features in the experimental phonon DOS can be assigned to specific groups of phonon modes. The motions of F atoms dominate the higher- and lower-energy parts of the DOS, and the majority of Sc-dominated modes are between 40 and 60 meV. The low-energy "rigid unit modes", where ScF_6 octahedra pivot about corner-shared F atoms, had negative Grüneisen constants (Fig. 3c), such as the low-energy modes at R and M with anomalous Grüneisen constants of –371 and –84. In what follows we show that these modes have quartic potentials, so these Grüneisen constants are not meaningful and the QHA is not reliable. Figure 4 shows the thermal expansion calculated with the QHA equation of state from Eq. 1, compared with the recent measurements [15]. Some difference at the highest temperatures could be caused by the creation of defects. For low temperatures, the QHA underestimates the NTE.

The ScF_6 octahedra are more flexible than their oxides counterparts – our MD simulations showed that the F atoms in an octahedron executed largely independent and uncorrelated motions, as shown in the animation, and by the radial and angular distribution functions in EPAPS document No. [number will be inserted by publisher]. At 300 K, the distributions of atom centers, projected onto one axis and binned into a histogram, were satisfactorily fit to Gaussian functions, giving full-width-half-maxima (FWHM) of 0.124 Å for Sc (isotropic) and 0.124 Å for F along the z-axis (longitudinal), and 0.270 Å for F along the x- and y-axes (transverse to the Sc-F bond) [number will be inserted by publisher]. The average transverse amplitude of the F-atom motion is more than 10 % of the Sc-F bond length at 300 K. We performed frozen phonon calculations for the five modes at the R-point. Most were fit well to a quadratic potential, but the R4+ mode (the mode of lowest energy calculated with the harmonic approximation), depicted in Fig. 5, was found to have a nearly pure quartic potential.

With the quasiharmonic model, analysis of the two bands of vibrations at 0−30 and 60−90 meV showed that they were dominated by the transverse and longitudinal motions of F atoms, respectively. The simple mechanical model of Fig. 1b, depicting the transverse motions of the F atoms, helps to show the important relationship between phonon anharmonicity and NTE. First consider the two Sc atoms in Fig. 1b to be positioned in equilibrium so there are no net forces on them when the F atom is at rest in mid-position ($x = 0$), as expected for a classical crystal with lattice parameter $2d$ at $T = 0$. For simplicity, first consider the Sc atoms rigidly positioned, as if they had infinite mass. The transverse restoring force on the F atom depends on the elongations of the springs, s, which goes as $1–\cos\theta$ times the resolved transverse force, giving a transverse restoring force going as x^3. The total potential for the transverse displacement of the F atom with two springs is

$$U_{\rm t} = \frac{k}{4}\frac{x^4}{d^2} \ , \qquad (2)$$

consistent with the quartic potential of the R4+ mode.

The force constant k was obtained from the frozen phonon calculations by fitting the transverse fluorine mode to a quartic function, and also by fitting the longitudinal fluorine mode to a quadratic function. The results, 901 and 744 N/m, respectively, are close. For these force constants the harmonic longitudinal vibrations of F atoms were 111 or 91.7 meV, reasonably close to the actual frequencies of these modes in the DOS.

From a numerical analysis of the quartic quantum oscillator [25], the $k = 901$ N/m gives energies of 7.4, 26.4, 51.9, 81.0, 113 meV for levels 0, 1, 2, 3, 4. The transition to the first excited state requires 19.0 meV, which is in good agreement with the peak 2 in the phonon DOS. The spread between these levels increases with temperature, so excitations to higher levels absorb increasingly more energy from the neutron, and peak 2 in Fig. 2 stiffens with temperature. This temperature dependence was calculated by assigning Boltzmann factors to the different oscillator levels, giving a shift of 7 meV over 750 K. This is about three times larger than the shift of peak 2, but peak 2 contains contributions from other phonon branches that are more harmonic. Next we allow for displacements of the Sc atoms and NTE. When the F atom is displaced transversely, the springs tend to pull the two Sc atoms together. The average displacements $\bar{x}_i$ of the F atoms at each energy level i were calculated numerically using quantum quartic wavefunctions. The average displacement $\bar{x}$ at temperature was then calculated by weighting $\{\bar{x}_i\}$ with level populations from Boltzmann distributions. The result in Fig. 4 shows many features of the experimental result of Greve [15], giving better agreement than the QHA.

Our frozen phonon calculations of modes with shape distortions of the octahedral ScF_6 units, but with fixed Sc-Fe first-nearest neighbor (1nn) distances, gave soft quadratic potentials, consistent with the Gaussian spread of F-atom displacements. The rocking of undistorted ScF_6 units about F-atom pivot points ("rigid unit modes") occurs without distortion of F-F 2nn distances, but these modes exist only on lines in the Brillouin zone

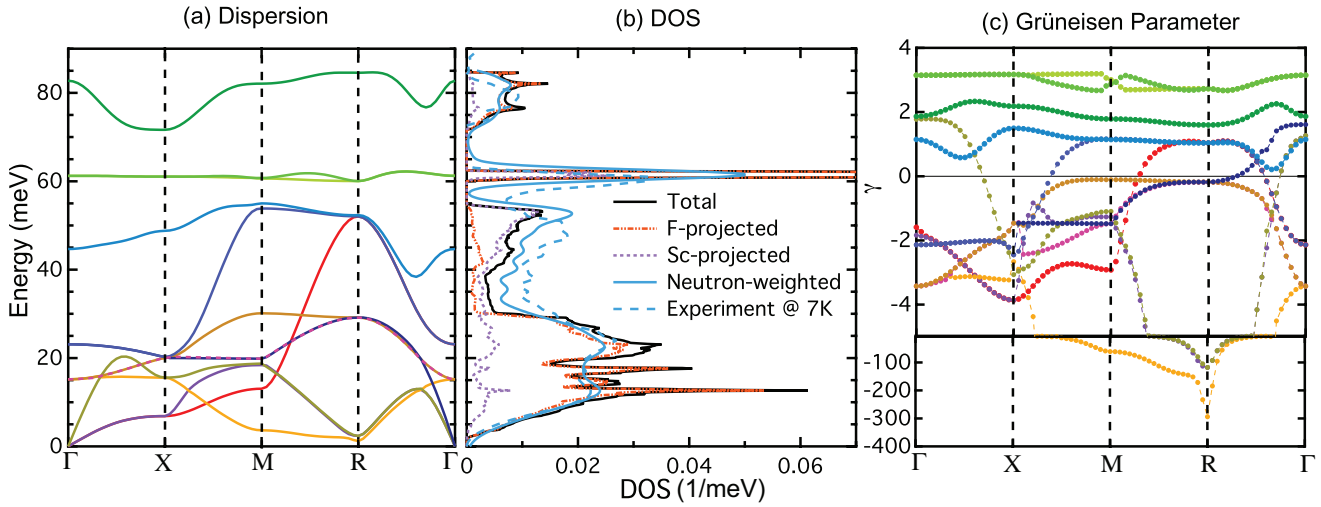

FIG. 3: (**a**) Calculated phonon dispersions along high symmetry directions of ScF_3 at 0 K. X = $(1,0,0)\pi/a$; M = $(1,1,0)\pi/a$; R = $(1,1,1)\pi/a$. (**b**) Total and partial phonon DOS curves at 0 K from first-principles calculation, neutron-weighted phonon DOS with instrument broadening at 120 meV added, and experimental neutron-weighted phonon DOS at 7 K. (**c**) Grüneisen parameters (γ) calculated with the QHA for modes along high symmetry directions. Colors correspond to the phonon dispersions in **a**.

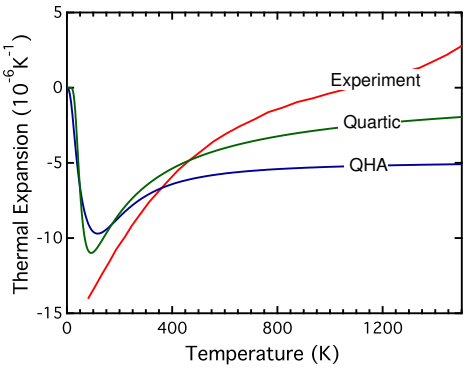

FIG. 4: Experimental [15] and calculated linear thermal expansion coefficients.

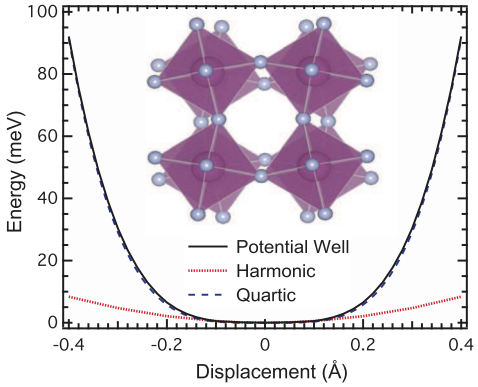

FIG. 5: Phonon mode R4+, its frozen phonon potential, quadratic (harmonic) and quartic fit to the frozen phonon potential. The range of the quadratic fit is from -0.1 to 0.1 Å for transverse displacements of F atoms.

along the M-R directions (the edges and corners of the cubic unit cell in reciprocal space). Nevertheless, with weak quadratic components, there are cylindrical volumes around these lines where the quartic potential dominates over the quadratic at modest temperatures. A full frozen phonon calculation for each mode in the Brillouin zone is not practical, but we obtained a volume in the Brillouin zone by setting a boundary where the QHA Grüneisen parameters were more negative than –5 [EPAPS]. For the R4+ modes centered around M-R, approximately two thirds of the Brillouin zone is within this anharmonic boundary, so there are a substantial number of modes with quartic behavior in ScF_3. The negative thermal expansion of ScF_3 should be a weighted combination of effects such as shown for the curves labeled QHA and Quartic in Fig. 4.

Although cubic ScF_3 transforms to a rhombohedral phase at a pressure of 0.6 GPa and then to another structure at about 3 GPa [18], the cubic DO_9 structure is robust over a wide range of temperature at ambient pressure. The phase stability could be explained by the large vibrational entropy from the large-amplitude fluorine motions responsible for NTE. A full analysis requires information on the lattice dynamics of the competing phases, of course.

The authors thank A. P. Wilkinson for important discussions. This work was supported by DOE BES under contract DE-FG02-03ER46055. The work benefited from software developed in the DANSE project under NSF award DMR-0520547. Research at Oak Ridge National Laboratory's SNS was sponsored by the Scientific User Facilities Division, BES, DOE.

* Electronic address: lichen@caltech.edu

[1] P. Söderlind, Europhys. Lett. **55 (4)**, 525 (2001).
[2] T. H. K. Barron, Ann. Phys. **1**, 77 (1957).
[3] A. W. Sleight, Curr. Opin. Solid St. M. **3**, 128 (1998).
[4] A. W. Sleight, Annu. Rev. Mater. Sci. **28**, 29 (1998).
[5] T. A. Mary *et al.*, Science **272**, 90 (1996).
[6] G. Ernst *et al.*, Nature **396**, 147 (1998).
[7] D. Cao *et al.*, Phys. Rev. Lett. **89**, 215902 (2002).
[8] J. N. Hancock *et al.*, Phys. Rev. Lett. **93**, 225501 (2004).
[9] M. G. Tucker *et al.*, Phys. Rev. Lett. **95**, 255501 (2005).
[10] G. D. Barrera *et al.*, J. Phys. Condens. Matter **17**, R217 (2005).
[11] Z. Schlesinger *et al.*, Phys. Rev. Lett. **101**, 015501 (2008).
[12] M. E. Simon and C. M. Varma, Phys. Rev. Lett. **86**, 1781 (2001).
[13] A. L. Goodwin and C. J. Kepert, Phys. Rev. B **71**, 140301 (2005).
[14] Giddy et al., Acta Cryst. **A49**, 697 (1993).
[15] B. K. Greve *et al.*, J. Am. Chem. Soc. **132 (44)**, 15496 (2010).
[16] M. Dapiaggi and A. N. Fitch, J. Appl. Crystallogr. **42**, 253 (2009).
[17] E. E. Rodriguez *et al.*, J. Appl. Phys. **105**, 114901 (2009).
[18] K. S. Aleksandrov *et al.*, Phys. Solid State **51**, 810 (2009).
[19] V. I. Zinenko and N. G. Zamkova, Phys. Solid State **42**, 1348 (2000).
[20] DRCS, http://danse.us/trac/DrChops (2010).
[21] M. Kresch *et al.*, Phys. Rev. B **77**, 024301 (2008).
[22] G. Kresse and J. Furthmüller, Comput. Mater. Sci. 6, 15 (1996); G. Kresse and J. Hafner, Phys. Rev. B **47**, 558 (1993); G. Kresse and J. Furthmüller, *ibid.* **54**, 11169 (1996).
[23] P. E. Blöchl, Phys. Rev. B **50**, 17953 (1994); G. Kresse and D. Joubert, *ibid.* **59**, 1758 (1999).
[24] K. Kunc and R. M. Martin, Phys. Rev. Lett. **48**, 406 (1982).
[25] P. Dorey and R. Tateo, J. Phys. A: Math. Gen. **32**, L419 (1999).